

The Threshold Anomaly of Optical Potentials and the Dispersion Relation for Weakly-bound Nuclear Systems

C. J. Lin* China Institute of Atomic Energy

E-mail: cjlin@ciae.ac.cn

**L. Yang, H. M. Jia, D. X. Wang, N. R. Ma, L. J. Sun, F. Yang, Z. D. Wu, X. X. Xu,
H. Q. Zhang and Z. H. Liu**

China Institute of Atomic Energy

Angular distributions of transfer reaction $^{208}\text{Pb}(^7\text{Li},^6\text{He})^{209}\text{Bi}$ were measured at $E_{\text{lab}}(^7\text{Li}) = 21.2, 24.3, 25.67, 28.55, 32.55, 37.55$ and 42.55 MeV. By fitting the experimental data with the theoretical frameworks of Distorted Wave Born Approximation (DWBA), the optical model parameters of halo nuclear system $^6\text{He} + ^{209}\text{Bi}$ were extracted. The breakup threshold anomaly (BTA) was observed clearly in the imaginary potential, and a further decreasing trend in the deep sub-barrier region was observed for the first time in a halo system. Furthermore, the dispersion relation is found of no use to describe the connection between the real and imaginary parts.

*The 26th International Nuclear Physics Conference
11-16 September, 2016
Adelaide, Australia*

*Speaker.

1. Introduction

The nuclear interaction is the most fundamental ingredient in the study of mechanisms of nuclear reactions. The optical model potential (OMP) is universally adopted to phenomenologically describe the interaction of nuclear collisions. With decades of researches on the OMPs of tightly bound systems, some basic properties of OMPs have been observed, *e.g.* when the interaction energy gets close to the Coulomb barrier, a strong energy dependence will be presented in both the real and imaginary parts due to the strong coupling between intrinsic degrees of freedom and reaction dynamics, which is known as the threshold anomaly (TA) [1, 2, 3, 4]. This behavior is characterized by a sharp decrease of the imaginary potential as the bombarding energy decreases towards the Coulomb barrier, associated with a localized bell-shaped structure around the barrier in the real part. The OMP can be written as

$$U(r; E) = V(r; E) + iW(r; E), \quad (1.1)$$

where the real potential $V(r; E)$ is composed of two parts,

$$V(r; E) = V_0(r; E) + \Delta V(r; E) \quad (1.2)$$

where the first term arises from the spatial nonlocality which is slowly and smoothly energy dependent in a large energy range, while the second term, named as dynamic polarization potential, is a consequence of the time nonlocality and links to the imaginary potential $W(r; E)$ with the dispersion relation,

$$\Delta V(r; E) = \frac{P}{\pi} \int_0^\infty \frac{W(r; E')}{E' - E} dE', \quad (1.3)$$

where P is the integrated principal value. The dispersion relation (known as the Kramers-Kronig relation in more general case) describes the effect of dispersion in a medium on the properties of a wave traveling within that medium and can be derived directly from the principle of causality.

Nowadays, with developments of facilities and detection technique of radioactive ion beams (RIBs), the OMPs of weakly bound systems have attracted great interests [5]. Compared with tightly bound systems, OMPs of these weakly bound systems will present some distinct properties, due to their exotic nuclear structure. A most significant feature is that, in the sub-barrier energy region, the depth of imaginary potential increases as the energy reduces. This abnormality indicates that even in the sub-barrier region, where the Coulomb repulsion effect is dominant, the absorption continues to be strong. This phenomenon strongly relates with the small breakup threshold of weakly bound system, thus it is so called the breakup threshold anomaly (BTA) [6, 7, 8]. However, due to the large data uncertainties [9], we are still far from the comprehensive understanding on the properties of the OMPs of weakly bound system, *e.g.* the increasing of the imaginary potential followed by a decreasing trend at sufficiently low energy region is barely observed [5, 10, 11], and the application of the dispersion relation is still debatable [3, 8, 12].

In view of this fact, we try to use the transfer reaction to study the OMPs of halo nuclear system. The greatest advantage of the transfer method is that the stable beam can be used to study the OMPs of halo system, yielding fairly high statistics. With this aim, the one-proton transfer reaction $^{208}\text{Pb}(^7\text{Li}, ^6\text{He})^{209}\text{Bi}$ was measured, to extract and study the OMPs of halo nuclear system $^6\text{He}+^{209}\text{Bi}$ as the exit channel [12].

2. Experiments

In order to make a complete understanding on the OMPs of ${}^6\text{He}+{}^{209}\text{Bi}$, two experiments were performed. Both of the experiments were carried out at the China Institute of Atomic Energy, Beijing, China. In the first experiment, the transfer reaction ${}^{208}\text{Pb}({}^7\text{Li}, {}^6\text{He}){}^{209}\text{Bi}$ within the near and above barrier region, where $E_{\text{lab}}({}^7\text{Li}) = 25.67, 28.55, 32.55, 37.55$ and 42.55 MeV were measured. While the second experiment is mainly focused on the near and sub-barrier energy region, and angular distributions of the transfer reaction with $E_{\text{lab}}({}^7\text{Li}) = 21.2, 24.3, 25.67, 28.55$ MeV were measured. In these two experiments, a ${}^{208}\text{Pb}$ target with thickness of about $120 \mu\text{g}/\text{cm}^2$ on a $20 \mu\text{g}/\text{cm}^2$ ${}^{12}\text{C}$ backing was bombarded by a ${}^7\text{Li}$ beam provided by the HI-13 tandem accelerator, with the current of about 40 pA. The setups for the two experiments are shown in Fig. 1. For the first measurement, the Q3D magnet spectrometer was used to detect the transfer reaction product, ${}^6\text{He}$. And a set of 7 Au(Si) surface barrier detectors were mounted in the chamber to measure the elastic scattering of ${}^7\text{Li}+{}^{208}\text{Pb}$. Because of the limit of angle coverage of Q3D spectrometer, two Si-detector telescopes were used in the second experiment to measure the transfer reaction, which were fixed at the backward angle region, with the angle coverage of $99^\circ - 127^\circ$ and $144^\circ - 171^\circ$, respectively. Each telescope contains three layers of Si-detectors, a $20 \mu\text{m}$ single-side strip detector (SSD, 16 channels), a $60 \mu\text{m}$ double-side strip detector (DSSD, 16×16 pixels), and a $1000 \mu\text{m}$ quadrant silicon detector (QSD) as the E_R detector. An array including 8 PIN detectors was also mounted to measure the elastic scattering of ${}^7\text{Li}+{}^{208}\text{Pb}$, with a coverage from 20° to 68° . Besides the silicon telescopes, 4 ion-chamber detect units were used to cover the forward and middle angle region. Each ion-chamber unit which is marked as IC in Fig. 1(b), contains one ionization chamber, followed by one DSSD with thickness of $500 \mu\text{m}$. The typical spectrum obtained by focal plane detector of Q3D spectrometer, as well as the silicon telescopes for the second experiment are shown in Fig. 2 and Fig. 3, respectively.

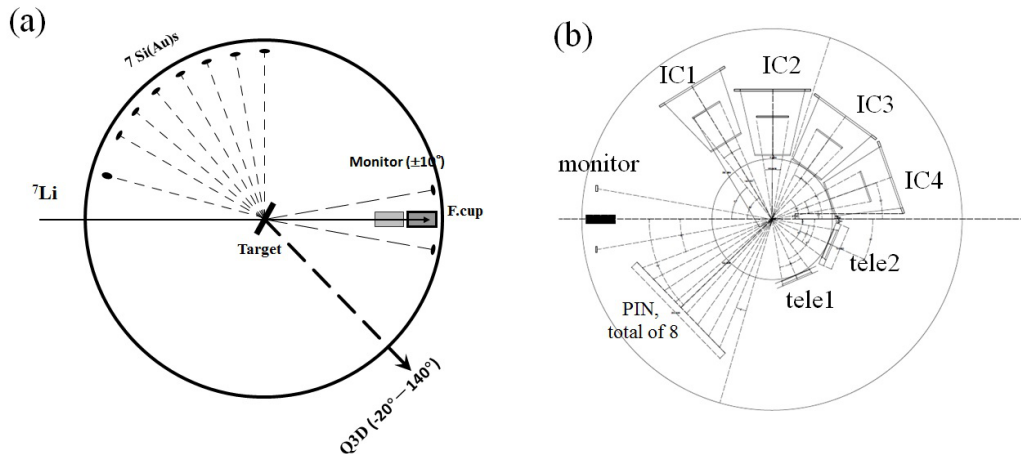


Figure 1: Setups for the first (a) and second (b) experiments. See the text for detail.

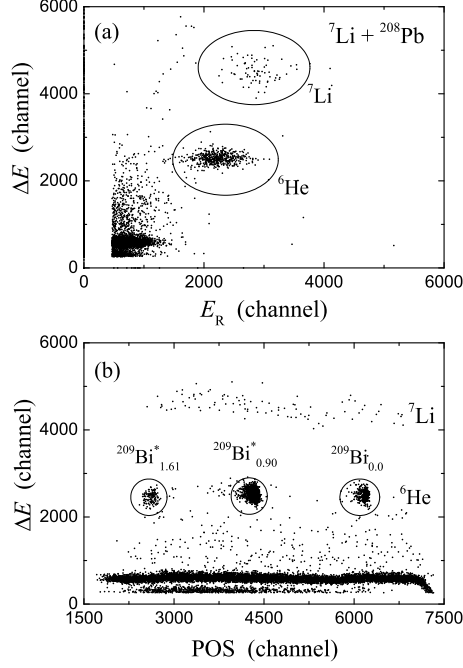


Figure 2: Typical spectrum recorded by the focal plane detector at $E_{\text{lab}} = 37.55$ MeV and $\theta_{\text{lab}} = 55^\circ$. The three groups of ${}^6\text{He}$ selected by circles correspond to the one-proton transfers to the ground, the first and the second excited states of ${}^{209}\text{Bi}$, respectively. This figure is taken from Ref. [12].

3. Results and discussions

The detail of experimental data, as well as the analysis procedure for the first measurement are already presented in Ref. [12]. While for the second experiment, the angular distributions of transfer reaction at the lowest two energies are shown in Fig. 4. The calculations were performed with the code of FRESKO [13]. The fitting results with DWBA method are also presented in Fig. 4 by solid curves. In the fitting process, the geometry parameters of the optical potential were fixed at $r_{0V} = 1.02$ fm, $a_V = 0.70$ fm, $r_{0W} = 1.25$ fm, and $a_W = 0.95$ fm [12]. Finally, the energy dependence of the strengths of real and imaginary parts at the sensitivity radius 13.5 fm is shown in Fig. 5, The errors of potential depths were derived by χ^2 analysis as described in Ref. [14], with a confidence level of 68.3%.

As shown in Fig. 5, strong energy dependence are observed for both the real and imaginary parts. For the imaginary part, according to the linear fitting result, the depth increases first as the interaction energy decreases in the sub-barrier region, demonstrating the BTA phenomenon clearly. With the energy reduced further, the depth of the imaginary potential begins to decrease. This is the first time that the decreasing trend in the imaginary potential is observed within a sufficient low energy region in a halo nuclear system. According to extrapolation of the linear fitting result, the

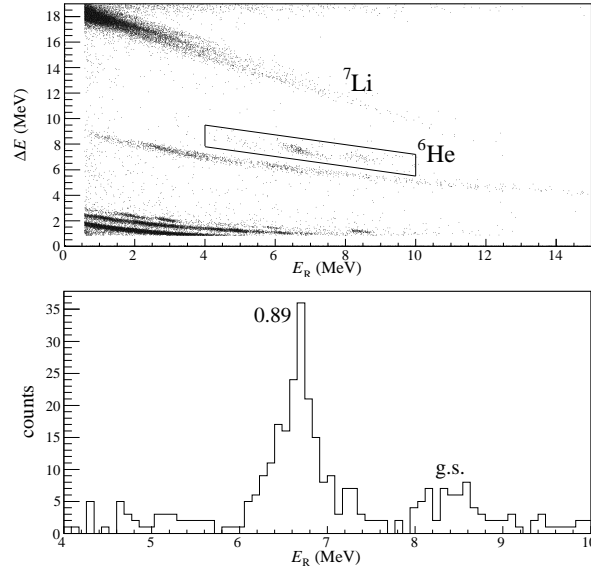


Figure 3: Typical spectrum obtained by the silicon telescope at $E_{\text{lab}} = 24.3$ MeV in the second experiment. The lower figure is the projected spectrum of selected ${}^6\text{He}$ band.

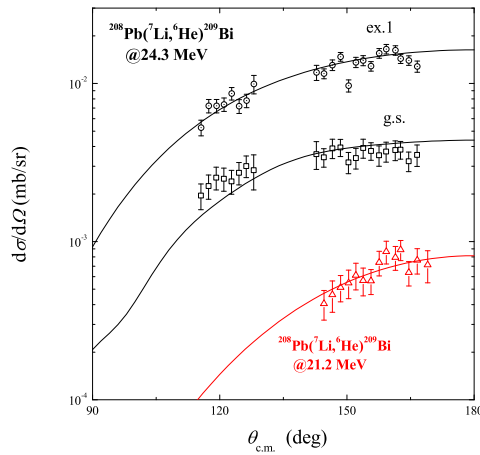


Figure 4: Angular distributions of ${}^{208}\text{Pb}({}^7\text{Li}, {}^6\text{He}){}^{209}\text{Bi}$ reactions for transferring to different excited states of ${}^{209}\text{Bi}$ at $E_{\text{lab}} = 21.2, 24.3$ MeV. The solid curves are the fitting results by DWBA.

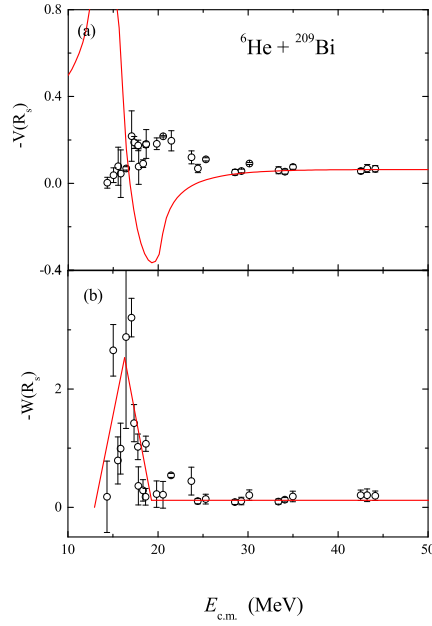


Figure 5: Energy dependence of the real (a) and imaginary (b) parts of the OMP at the sensitivity radius of 13.5 fm. The solid curves in (b) show the linear segment fitting results for the imaginary potential. The solid curve in (a) presents the calculation result for the real potential according to the dispersion relation with the variation of the imaginary part.

reaction threshold energy, where the imaginary potential vanishes, can be derived, as about $0.73V_B$. This threshold indicates that all the non-elastic channels are effectively closed by the Coulomb barrier, and reactions occur only when the interaction energy gets above this threshold energy to overcome the repulsive Coulomb barrier.

On the other hand, the applicability of the dispersion relation is investigated for this halo nuclear system. The calculation result for the real potential according to the dispersion relation with the variation of the imaginary potential is shown in Fig. 5 (a). The calculation result demonstrates clearly that the dispersion relation can not describe the trend of real potential correctly, indicating that the dispersion relation does not hold for the weakly bound system. However, in Refs. [6, 8] the authors still tried to use the dispersion relation to describe the connection between the real and imaginary parts of the OMPs of weakly bound systems. Due to large uncertainties of the results, it is hardly to draw a specific conclusion. Therefore, whether the dispersion relation is suitable for the weakly-bound system is still an open question, and deserves further investigation.

Acknowledgments

This work is supported by the National Key Basic Research Program of China (No. 2013CB834404), and the National Natural Science Foundation of China under Grants Nos. 11505293, 11375268,

11475263, U1432246, U1432127, 11635015.

References

- [1] M. A. Nagarajan, C. C. Mahaux, and G. R. Satchler, *Phys. Rev. Lett.* **54**, 1136 (1985).
- [2] B. R. Fulton, D. W. Banes, J. S. Lilley *et al.*, *Phys. Lett. B* **162**, 55 (1985).
- [3] C. Mahaux, H. Ngo, and G. R. Satchler, *Nucl. Phys. A* **449**, 354 (1986).
- [4] G. R. Satchler, *Phys. Rep.* **199**, 147 (1991).
- [5] L. F. Canto, P. R. S. Gomes, R. Donangelo *et al.*, *Phys. Rep.* **596**, 1 (2015).
- [6] A. R. Garcia, J. Lubian, I. Padron *et al.*, *Phys. Rev. C* **76**, 067603 (2007).
- [7] N. Keeley, S. J. Bennett, N. M. Clarke *et al.*, *Nucl. Phys. A* **571**, 326 (1994).
- [8] M. S. Hussein, P. R. S. Gomes, J. Lubian and L. C. Chamon, *Phys. Rev. C* **73**, 044610 (2006).
- [9] C. Signorini, A. Andrighetto, M. Ruan *et al.*, *Phys. Rev. C* **61**, 061603(R) (2000).
- [10] L. Fimiani, J. M. Figueira, G. V. Marti *et al.*, *Phys. Rev. C* **86**, 044607 (2012).
- [11] J. M. Figueira, J. O. Fernandez Niello, A. Arazi *et al.*, *Phys. Rev. C* **81**, 024613 (2010).
- [12] L. Yang, C. J. Lin, H. M. Jia *et al.*, *Phys. Rev. C* **89**, 044615 (2014).
- [13] I. J. Thompson, *Comp. Phys. Rep.* **7**, 167 (1988).
- [14] D. Abriola, A. Arazi, J. Testoni *et al.*, *J. Phys.: Conf. Ser.* **630**, 012021 (2015).